Featured in Physics

Coulomb Screening of Superconductivity in Magic-Angle Graphene

Julien Barrier,[1,2,*] Liangtao Peng,[3] Shuigang Xu,[2] Christophe De Beule,[4,5] V. I. Fal'ko,[1,2,6] K. Watanabe,[7] T. Taniguchi,[7] A. K. Geim,[1,2,§] Shaffique Adam,[3,8,‡] and Alexey I. Berdyugin[8,9,1,†]

[1]School of Physics and Astronomy, University of Manchester, Manchester M13 9PL, United Kingdom
[2]National Graphene Institute, University of Manchester, Manchester M13 9PL, United Kingdom
[3]Department of Physics, Washington University in St. Louis, St. Louis, Missouri 63130, USA
[4]Department of Physics and Astronomy, University of Pennsylvania, Philadelphia, Pennsylvania 19104, USA
[5]Department of Physics, University of Antwerp, Groenenborgerlaan 171, 2020 Antwerp, Belgium
[6]Henry Royce Institute for Advanced Materials, The University of Manchester, Oxford Road, Manchester, M13 9PL, United Kingdom
[7]National Institute for Materials Science, 1-1 Namiki, Tsukuba 305-0044, Japan
[8]Department of Materials Science and Engineering, National University of Singapore, 9 Engineering Drive 1, Singapore 117575, Singapore
[9]Department of Physics, National University of Singapore, 2 Science Drive 3, Singapore 117551, Singapore

(Received 3 November 2025; revised 20 February 2026; accepted 9 June 2026; published 17 August 2026)

The origin of superconductivity in magic-angle twisted bilayer graphene has been a subject of intense debate. While some experimental evidence indicated an unconventional pairing mechanism which should be sensitive to Coulomb screening, experimental attempts to tune the critical temperature by screening Coulomb interactions so far have remained unsuccessful, possibly indicating a conventional phonon-mediated pairing. Here we study a double-layer electronic system consisting of two twisted graphene bilayers in immediate proximity of each other but remaining electronically decoupled. By increasing the carrier density in one bilayer, we completely suppressed both the superconductivity and the correlated-insulator state in the adjacent magic-angle graphene. The observation of such an effect from screening offers support for an unconventional mechanism of Cooper pairing in magic-angle twisted bilayer graphene, shedding new light on the underlying physics governing their properties.

DOI: 10.1103/z9qg-287y

Subject Areas: Condensed Matter Physics, Semiconductor Physics, Superconductivity

I. INTRODUCTION

Superconductivity in magic-angle twisted bilayer graphene (TBG) has attracted an intense interest [1–14] due to its presumed unconventional origin. This belief stems from several experimental observations including the combination of a relatively low carrier density with an unusually high critical temperature [5], and the striking resemblance between magic-angle TBG's phase diagram and that of Cuprate superconductors [5,6]. Also, the maximum of the critical temperature T_C roughly coincides with the "magic angle" of 1.1° between graphene layers [7,11] where the flattened energy bands maximize electron-electron interactions [15], suggesting that they may play a critical role in Cooper pairing. These observations have spurred numerous theories for unconventional mechanisms including plasmon-mediated [16–18], skyrmion-mediated [19,20], Kohn-Luttinger [21,22], and nodal pairing-enabled mediated by intervalley coherent state [23] mechanisms. However, other studies remain supportive of the conventional phonon-mediated pairing [10–14,24–28].

Further efforts to clarify the pairing mechanism have so far been inconclusive. While certain findings (e.g., a V-shaped differential conductance in tunnelling spectra [8] and the observed interaction-driven superfluid stiffness with a small superconducting coherence length [9] support an unconventional pairing mechanism, experiments employing proximity screening point towards a phonon-mediated superconductivity [10–12]. The latter

*Present address: Max Planck Institute for Solid State Research, D-70569 Stuttgart, Germany.
†Contact author: alexey@nus.edu
‡Contact author: shaffique@wustl.edu
§Contact author: geim@manchester.ac.uk

experiments initially employed gates made of graphite to provide electrostatic screening of Coulomb interactions inside magic-angle TBG. The gates were separated by thin (6–10 nm) hexagonal boron nitride (hBN) spacers [11,12]. It was found that the screening suppressed correlated insulator (CI) states, while superconductivity persisted. However, the differing behaviors of CI and superconductivity in these experiments could arise from the variations of twist angle between different devices, with superconductivity surviving in a broader range of twist angles [11], complicating the interpretation. Moreover, it was impossible to measure the change of the superconducting critical temperature T_C induced by the screening within a same device, as the screening was generally fixed by graphite's density of states and by the thickness of the dielectric spacer, while devices with different spacers inevitably had different twist angles. A more recent experiment employed Bernal bilayer graphene as a tunable screening layer that was decoupled from magic-angle TBG by thinner, 3-nm-thick hBN [10]. While screening again suppressed CI states, T_C increased by 2–3%. This marginal increase was interpreted as a sign of conventional superconductivity where the screening suppressed Coulomb repulsion between electrons forming phonon-coupled Cooper pairs.

In contrast with previous experiments, the present work demonstrates a complete suppression of magic-angle superconductivity with tunable screening, with variations in T_C by more than an order of magnitude, which is an attribute of unconventional pairing. As the screening efficiency of the metallic layer decays exponentially at distances as small as ~1–2 nm [29], we maximized the screening by using a double-layer electronic system consisting of two small-angle TBG layers stacked directly on top of each other. Instead of using a thin dielectric spacer, we employed a high twist angle between the two TBG layers, which is sufficient to decouple their electronic systems [30–37]. The high-twist angle configuration effectively allowed a sub-nm separation between the magic-angle TBG and the screening layer, enhancing the screening efficiency in our device. Our devices demonstrate a new experimental architecture to combine different twisted layers within the stack, while allowing the controllable interplay between their properties.

II. RESULTS

To create a double-layer electronic system, we assembled twisted tetralayer graphene using the twist angle sequence shown in Fig. 1(a). Briefly, the first two layers were rotated relative to each other at an angle of ~1°, the third layer was rotated at ~10° relative to the second, and the fourth layer was rotated again at ~0.5° relative to the third. This multitwisted graphene stack was then encapsulated between thick (30 nm) hBN crystals to preserve graphene's electronic quality and placed on a silicon oxide substrate [38]. Its longitudinal ρ_{xx} and Hall ρ_{xy} resistivities are plotted in Figs. 1(b) and 1(c) as a function of carrier densities induced by top and bottom gates [38]. The observed multiple peaks in ρ_{xx} correlate with peaks and sign changes in ρ_{xy}. This behavior is attributed to the formation of electronic minibands inside each of the twisted bilayers forming the tetralayer stack, as expected for small twist angles.

To probe the electronic structure of our tetralayer, we measured its resistivity as a function of both gate voltages [Fig. 1(d)]. This map revealed two distinct sets of peaks. One set [red arrows in Fig. 1(d)] depended primarily on the density n_{bg} induced by the bottom gate and showed little sensitivity to the top gate-induced density n_{tg}. The other set (blue arrows) responded mostly to n_{tg} with weak response to n_{bg}. The observed peaks in ρ_{xx} are attributed to main and secondary neutrality points (NPs) within the miniband structure of the bottom and top TBGs with small twist angles. Indeed, it is expected that the bottom gate mainly affects the carrier density in the bottom TBG and does not affect the top TBG because of screening, and vice versa for the top gate. However, the gate-induced carrier densities were distributed between both TBG layers, as detailed in [38]. We note that such behavior is a simple electrostatic

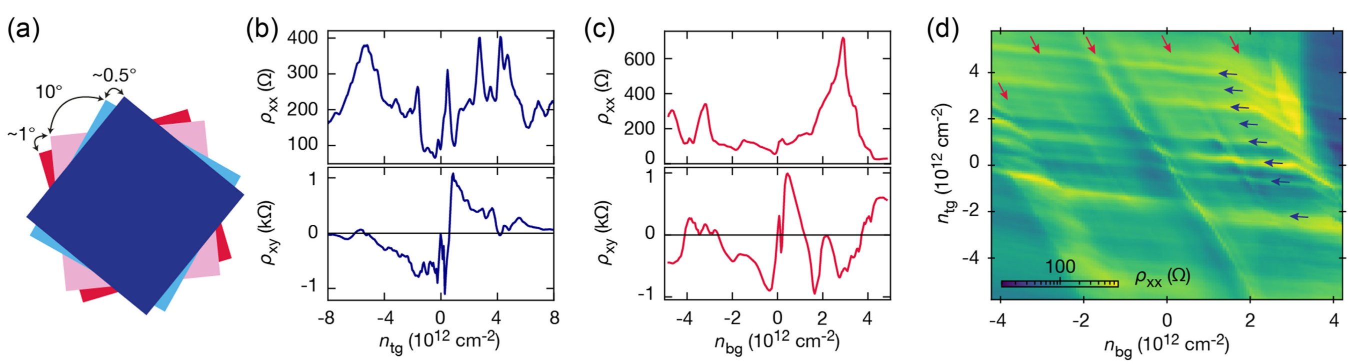

FIG. 1. Characterization of twisted tetralayer graphene device. (a) Schematics of its structure. (b) and (c) Longitudinal and Hall resistivities (top and bottom panels, respectively) as a function of top (b) and bottom (c) gate-induced carrier densities. Panel (b) was measured for $n_{bg} = 0$, and panel (c) for $n_{tg} = 0$. The Hall signal was antisymmetrized using small magnetic fields of ±100 mT. (d) Longitudinal resistivity as a function of n_{tg} and n_{bg}. All measurements at 2 K.

effect, which does not imply the coupling between the layers.

To accurately determine the carrier density inside top and bottom TBG layers (n_{tTBG} and n_{bTBG}, respectively), we analyzed the ρ_{xx} maps (see Supplemental Material [38]). The resulting resistivity map using the new density coordinates (n_{bTBG} and n_{tTBG}) is shown in Fig. 2(a). In this representation, the peaks attributed to NPs in the bottom TBG form vertical lines, and the ones attributed to the top TBG form horizontal lines. This shows that the electronic structure of our graphene tetralayer can be understood in terms of two independent electronic systems [38], in agreement with the experimental design. Then, it becomes straightforward to evaluate the twist angles θ for the two TBG layers. Considering that the full filling of each miniband corresponds to 4 electrons per superlattice unit cell, the carrier density at which the secondary NPs occurred is given by $n = 4/A$, where $A = \sqrt{3}a^2/8\sin^2(\theta/2)$ is the unit cell area, and a is graphene's lattice constant. Applying this expression to the carrier density difference between the most pronounced vertical and horizontal resistivity peaks in Fig. 2(b), we obtained twist angles $\theta_{\mathrm{bTBG}} = 1.15°$ and $\theta_{\mathrm{tTBG}} = 0.46°$ for the bottom and top TBG, respectively. These twist angles also agree well with the observed positions of Brown-Zak oscillations [38]. The twist angle of the bottom TBG is within the range for magic angle [1–14] while the top TBG's small angle allows a rather high density of states (DOS) which is important for achieving a high screening efficiency (see below).

After determining θ, we analyzed the tetralayer's electronic behavior in more detail. In Fig. 2(a), apart from the pronounced vertical maxima at n_{bTBG} around zero and $\pm 3 \times 10^{12}$ cm^{-2} which correspond to zero ($\nu = 0$; main NP) and full filling ($\nu = \pm 4$; secondary NPs) of the first miniband of the bottom TBG (ν is the number of electrons per unit cell), there is also a weaker structure that emerged around $\nu = \pm 2$. We attributed those peaks to the CI states, as reported previously for magic-angle TBG [1–6,8–12]. These states were sensitive to doping of the top TBG and completely disappeared once n_{tTBG} exceeded 2×10^{12} cm^{-2} as shown in Fig. 2. The decoupling between the two TBGs was corroborated from the absence of signatures of moiré imprinting [38]. In such case, one would expect to observe additional peaks at constant n_{bTBG}, at similar carrier densities at which peaks are observed in the top TBG layer. No such features were observed confirming that the two TBG layers were decoupled using large twist angles.

To check for the presence of superconductivity, we measured the same map $\rho_{xx}(n_{\mathrm{bTBG}}, n_{\mathrm{tTBG}})$ at our lowest temperature T of ~35 mK [Fig. 3(a)]. The main difference with respect to the 2 K map of Fig. 2(a) is the zero resistivity regions that appeared around $\nu = \pm 2$ in the magic-angle bottom TBG [also, compare Figs. 2(b) and 3(b)]. The

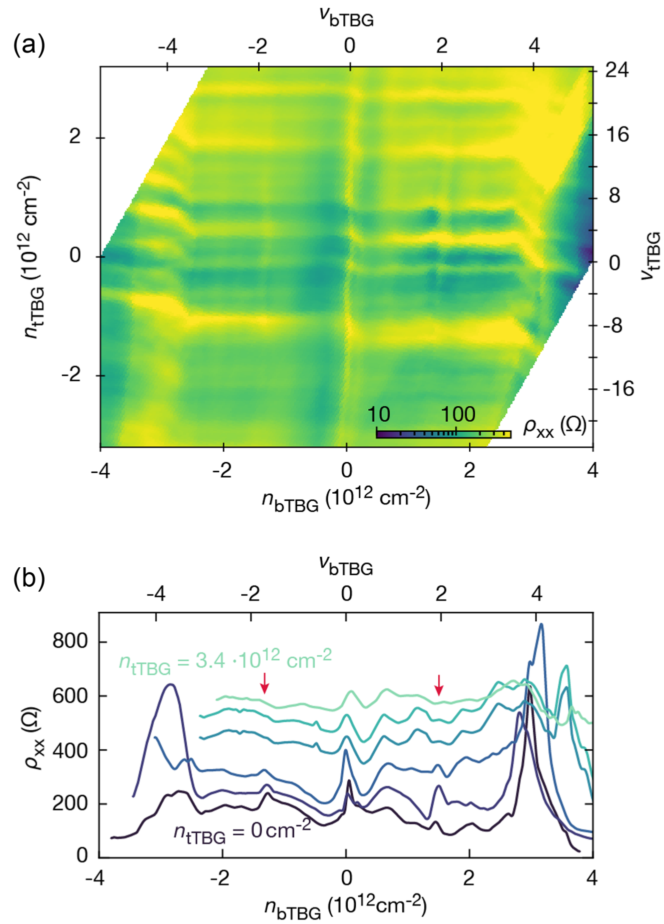

FIG. 2. Tuning magic-angle correlated states with top-layer density. (a) Longitudinal resistivity as a function of the calculated carrier densities in top and bottom TBGs. Notable curving at intersections of vertical and horizontal high resistivity states are caused by changes in screening, which are most pronounced if the Fermi level crosses a gapped state inside one of the TBG layers [38]. (b) Line cuts from panel (a), showing resistivity for fixed carrier densities in the top TBG layer. For clarity, the curves are offset vertically in steps of 0.68×10^{12} cm^{-2}. Curves without offset are shown in Fig. S3 [38]. The red arrows indicate positions of the resistivity peaks around $\nu = \pm 2$ which disappear upon increasing the carrier density in the top TBG. All measurements at 2 K. The increase in resistance observed in the top-right corner of panel (a) [see also Fig. 1(d)] around filling factor 4 of the bottom TBG layer can most likely be attributed to the increased resistance of the voltage probes located outside the region covered by the top gate, as highlighted in Fig. S1 [38].

zero-resistance states quickly disappeared if ν was tuned away from ± 2. The states also disappeared with increasing T [Fig. 3(c)], and upon increase of a dc current I_{dc} [Fig. 3(d)]. This behavior is characteristic of the superconductivity previously reported for magic-angle graphene [1–12]. Unexpectedly, the superconductivity was also suppressed if the carrier density in the top TBG layer increased [Fig. 3(a)]. This is further illustrated in Figs. 3(d) and 3(e), which show changes in T_{C} and the critical current as a function of n_{tTBG}. Such suppression cannot be

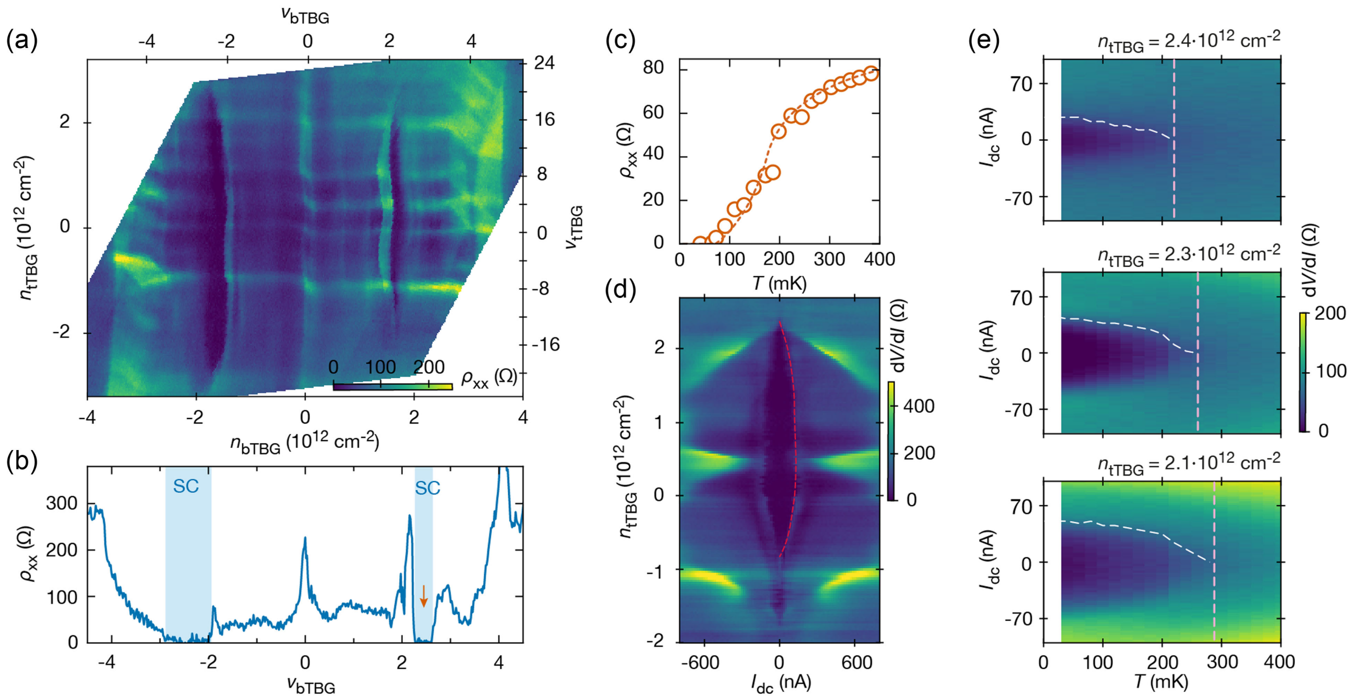

FIG. 3. Screening of magic-angle superconductivity. (a) Longitudinal resistivity as a function of carrier density in the top and bottom TBGs at 35 mK. Same color scale as in Fig. 1(e). (b) ρ_{xx} as a function on n_{bTBG} measured at zero n_{tg}. (c) Temperature dependence of ρ_{xx} at the density indicated by the arrow in panel (b). Dashed curve, guide to the eye. At zero top-gate voltage, increased contact resistivity leads to a slightly reduced T_C compared with panel (e) at higher carrier density. All other measurements were performed under applied top-gate voltage (Fig. S10 [38]). (d) Differential resistance as a function of I_{dc} and n_{tTBG} for the same n_{bTBG} as in panel (c). Red dashed line is a guide to the eye highlighting superconducting critical current. The asymmetry critical currents range for positive and negative n_{tTBG} possible originate from the asymmetry in the band structure of the top TBG layer. The additional arclike pattern which appears at high current can be attributed to the out-of-equilibrium criticalities in one of the TBG layers [83]. A magnified view at lower bias currents is presented in Fig. S20 [38]. (e) Differential resistance as a function of I_{dc} and T for different n_{tTBG}. The arclike dashed curves mark the critical current defined as the current at which ρ_{xx} reaches half the normal-state resistivity. The vertical lines mark T_C.

attributed to the simultaneously changed displacement field within the bottom TBG layer and requires an alternative explanation [38].

III. DISCUSSION

The changes in the bottom TBG induced by doping of the top TBG may originate from two distinct mechanisms. First, the metallic top TBG layer may short conduction pathways at higher $|n_{tTBG}|$ and reduce the correlated insulator gap. However, the sample's resistivity does not decrease at high doping levels of the top TBG layer [see Fig. 2(a)], as would be expected from a parallel conduction mechanism. Second, the top TBG layer may modify the electrostatic potential and tune the magnitude of Coulomb interactions within the stack. Since the large twist angle between the TBG layers decouples their electronic band structures, we attribute the changes in the properties of the bottom TBG induced by doping of the top TBG to the modified Coulomb interaction within the stack. Earlier reports [10–12] also demonstrated that screening of Coulomb interactions in magic-angle TBG reduces the CI state's gap. Based on these conclusions we also attribute the suppression of the CI states around $\nu = \pm 2$ [Figs. 2 and 3(a)] to increased screening efficiency of the top TBG as its doping increased. On the other hand, T_C in the earlier experiments was either unaltered by screening [11,12] or only marginally (~2%) increased [10]. In stark contrast, T_C in our experiment was so strongly affected by screening that superconductivity could be destroyed even at our lowest T [Figs. 3(a), 3(d), and 3(e)]. We believe that the critical difference between our and earlier experiments is the distance l between the screening layer and the magic-angle TBG. In our case, l was sub-nm, that is 1 order of magnitude smaller than previously. While l of several nm is sufficient to suppress the CI state, the screening of superconductivity poses stronger requirements. As shown in Ref. [38] for the half-filled miniband supporting magic-angle superconductivity, the screening efficiency decays exponentially over a characteristic distance of ~2 nm. In addition, the DOS of our top small-angle TBG is expected to be higher than that of the Bernal-stacked bilayer graphene employed previously, which also enhances the screening efficiency (Fig. S17 [38]).

For further analysis, we calculated the Coulomb interaction in the bottom TBG as $V_{\mathrm{bTBG}}(\boldsymbol{q},\omega) = V_0/\epsilon$, where V_0 is the bare Coulomb interaction, and ϵ is the dielectric function of our four-layer system, which can be written as $\epsilon = \beta - V_0\,\Pi_{\mathrm{bTBG}}$. Here, β is the screening contribution from the top layer, and Π_{bTBG} is the intralayer polarizability of magic-angle TBG. The interlayer screening term β depends on l and, in the limit $l \to 0$, β becomes proportional to the dielectric constant of the top layer, which is set by an average DOS around the Fermi energy [38]. Conversely, if l becomes comparable with the magic-angle superlattice period, β approaches 1 so that the top TBG no longer contributes to screening of Coulomb interactions. To evaluate β, one needs to know the DOS of the screening (top) layer. For this purpose, we performed band structure calculations using different theoretical models that incorporate lattice relaxation, strain, and intralayer Coulomb interactions, all of which are important in marginally twisted bilayers. The results are shown in Fig. S19 [38]. We find that the magnitude of DOS and its behavior at high carrier densities are highly sensitive to the modelling assumptions, which renders predictions unreliable.

Nevertheless, a model may capture the qualitative trends observed in our experiment by satisfying two essential criteria: (1) an increasing DOS with the carrier density and (2) the DOS's order of magnitude should be consistent with experimental observations. To avoid over-modelling, we chose to simplify the problem and approximate the DOS of the top TBG layer $\mathcal{N}_{\mathrm{tTBG}}$ as a scaled single-layer graphene band structure, characterized by a scaling factor α. We model it as $\mathcal{N}_{\mathrm{tTBG}} = \alpha \times \mathcal{N}_{\mathrm{Gr}}$ where $\mathcal{N}_{\mathrm{Gr}}$ is the DOS of monolayer graphene. The proportionality coefficient α can be estimated by modelling the suppression of the CI state in a way that the CI gap becomes smaller than 2 K if the carrier density in the top TBG layer exceeds $2 \times 10^{12}\ \mathrm{cm}^{-2}$, as per our experiment (Fig. 2). Further details are discussed in Ref. [38]. This simple estimation gives $\alpha \sim 10$, which is just a factor of two away from the top TBG DOS obtained using sophisticated models accounting for the lattice relaxation, and intralayer Coulomb interactions at the characteristic carrier density $2 \times 10^{12}\ \mathrm{cm}^{-2}$ (see Fig. S18 [38]). Given the complexity of the problem, we believe this level of agreement is reasonable and supports the validity of our simplified approach.

Using the modeled $\mathcal{N}_{\mathrm{tTBG}}$, we could estimate how different mechanisms of superconductivity would be affected by the proximity screening. In conventional superconductors, where electron-electron repulsion is stabilized by phonon-induced attraction, the screening should generally suppress the repulsion and, hence, increase T_{C} [10], which contradicts our observations. In principle, the screening might also affect the deformation potential and reduce the electron-phonon coupling. This scenario is considered in Ref. [38] and shown to be unrealistic. Accordingly, the screening behavior observed in our experiment rules out the conventional (BCS-like) mechanisms of Cooper pairing and lends support to an electronic pairing mechanism. As an example of the latter mechanisms, we considered electron-plasmon pairing [16–18] for which screening is expected to strongly impact superconductivity [17,18]. Our numerical modeling shows that, indeed, screening by the top TBG should greatly reduce T_{C} [38]. The comparison between critical temperatures observed in experiment and modeling results is shown in Fig. S10 [38]. Furthermore, we find that in this mechanism the critical temperature is sensitive to the average DOS of the screening layer over a broad energy window, rather than to its precise value at the Fermi level [38]. This explains the absence of pronounced modulation of critical temperature and the critical current near the CNPs of the top TBG layer, where the DOS exhibits a local minimum. Finally, we numerically calculated the dependence T_{C} (l) for this particular pairing mechanism and found that the screening effect should be most pronounced at sub-nm distances and rapidly decrease with increasing l above $\sim$2 nm, in agreement with the exponential dependence derived in Ref. [38].

Although our modeling using a plasmon-induced pairing yields reasonable agreement with the experimental observations, a complete theoretical treatment would require a fully self-consistent GW calculation of the entire four-layer system, which is technically unfeasible at this point. Additionally, we point out that, while plasmon-mediated superconductivity seems a plausible explanation for magic-angle superconductivity, we cannot rule out other unconventional mechanisms such as, e.g., skyrmion-mediated [19,20], Kohn-Luttinger [21,22], and nodal pairing-enabled mediated by inter-valley coherent states [23]. The latter mechanisms are similarly susceptible to proximity screening. Finally, we considered the possibility that the observed destruction of superconductivity originates from the reversed proximity effect [84] between the magic-angle superconductor and the normal-metal top TBG. This scenario would require a highly transparent superconductor-normal metal interface, which is not the case with our system [38].

IV. CONCLUSIONS

Our experiments revealed a striking sensitivity of the magic-angle superconductivity to proximity screening, which seems to rule out conventional phonon pairing and tightens constraints on possible unconventional mechanisms of superconductivity in magic-angle TBG. Additionally, our approach of combining small and large twist angles within the same heterostructure shows a way to design novel electronic systems where Coulomb interactions in one layer are screened by controlling the carrier density in the other. Looking ahead, in future work it would be interesting to combine superconducting magic-angle TBG or other flat-band systems with monolayer graphene, exploiting the more controllable and well-characterised density of states of the screening layer. Finally, we note that while conceptually similar to previously studied double-layer systems separated by thin dielectric spacers [85–87], the high-twist-angle approach provides ultimately small separation between electronic systems, which is essential for efficient screening, and could also be used to explore inter- and intralayer interaction effects in moiré quantum materials [1,2,88].

Note added. Recently, we became aware of another work sharing the same conclusion on the role of screening in magic-angle TBG [89].

ACKNOWLEDGMENTS

We acknowledge financial support from the Lloyds Register Foundation, ERC and UKRI (Grant No. 2XPLO2D) and the Royal Society. L. P., C. D. B., and S. A. acknowledge a start-up grant from Washington University in St. Louis. This work has been supported by the National Research Foundation, Singapore under its NRF Fellowship (NRFF) (NRF-NRFF16-2024-0011), and by A*STAR under its RIE2025 Manufacturing, Trade and Connectivity (MTC) Young Individual Research Grant (M23M7c0126) awarded to A. I. B

DATA AVAILABILITY

The data are available upon reasonable request from the authors.

[1] L. Balents, C. R. Dean, D. K. Efetov, and A. F. Young, *Superconductivity and strong correlations in moiré flat bands*, Nat. Phys. **16**, 725 (2020).

[2] C. N. Lau, M. W. Bockrath, K. F. Mak, and F. Zhang, *Reproducibility in the fabrication and physics of moiré materials*, Nature (London) **602**, 41 (2022).

[3] X. Lu *et al.*, *Superconductors, orbital magnets and correlated states in magic-angle bilayer graphene*, Nature (London) **574**, 653 (2019).

[4] M. Yankowitz, S. Chen, H. Polshyn, Y. Zhang, K. Watanabe, T. Taniguchi, D. Graf, A. F. Young, and C. R. Dean, *Tuning superconductivity in twisted bilayer graphene*, Science **363**, 1059 (2019).

[5] Y. Cao, V. Fatemi, S. Fang, K. Watanabe, T. Taniguchi, E. Kaxiras, and P. Jarillo-Herrero, *Unconventional superconductivity in magic-angle graphene superlattices*, Nature (London) **556**, 43 (2018).

[6] Y. Cao, D. Chowdhury, D. Rodan-Legrain, O. Rubies-Bigorda, K. Watanabe, T. Taniguchi, T. Senthil, and P. Jarillo-Herrero, *Strange metal in magic-angle graphene with near Planckian dissipation*, Phys. Rev. Lett. **124**, 076801 (2020).

[7] Y. Cao, D. Rodan-Legrain, J. M. Park, N. F. Q. Yuan, K. Watanabe, T. Taniguchi, R. M. Fernandes, L. Fu, and P. Jarillo-Herrero, *Nematicity and competing orders in superconducting magic-angle graphene*, Science **372**, 264 (2021).

[8] M. Oh, K. P. Nuckolls, D. Wong, R. L. Lee, X. Liu, K. Watanabe, T. Taniguchi, and A. Yazdani, *Evidence for unconventional superconductivity in twisted bilayer graphene*, Nature (London) **600**, 240 (2021).

[9] H. Tian *et al.*, *Evidence for Dirac flat band superconductivity enabled by quantum geometry*, Nature (London) **614**, 440 (2023).

[10] X. Liu, Z. Wang, K. Watanabe, T. Taniguchi, O. Vafek, and J. I. A. Li, *Tuning electron correlation in magic-angle twisted bilayer graphene using Coulomb screening*, Science 2021) 1261 ,**371**).

[11] Y. Saito, J. Ge, K. Watanabe, T. Taniguchi, and A. F. Young, *Independent superconductors and correlated insulators in twisted bilayer graphene*, Nat. Phys. **16**, 926 (2020).

[12] P. Stepanov, I. Das, X. Lu, A. Fahimniya, K. Watanabe, T. Taniguchi, F. H. L. Koppens, J. Lischner, L. Levitov, and D. K. Efetov, *Untying the insulating and superconducting orders in magic-angle graphene*, Nature (London) **583**, 375 (2020).

[13] Y. Saito, F. Yang, J. Ge, X. Liu, T. Taniguchi, K. Watanabe, J. I. A. Li, E. Berg, and A. F. Young, *Isospin Pomeranchuk effect in twisted bilayer graphene*, Nature (London) **592**, 220 (2021).

[14] H. Polshyn, M. Yankowitz, S. Chen, Y. Zhang, K. Watanabe, T. Taniguchi, C. R. Dean, and A. F. Young, *Large linear-in-temperature resistivity in twisted bilayer graphene*, Nat. Phys. **15**, 1011 (2019).

[15] R. Bistritzer and A. H. MacDonald, *Moiré bands in twisted double-layer graphene*, Proc. Natl. Acad. Sci. U.S.A. **108**, 12233 (2011).

[16] G. Sharma, M. Trushin, O. P. Sushkov, G. Vignale, and S. Adam, *Superconductivity from collective excitations in magic-angle twisted bilayer graphene*, Phys. Rev. Res. **2**, 022040(R) (2020).

[17] C. Lewandowski, D. Chowdhury, and J. Ruhman, *Pairing in magic-angle twisted bilayer graphene: Role of phonon and plasmon umklapp*, Phys. Rev. B **103**, 235401 (2021).

[18] L. Peng, I. Yudhistira, G. Vignale, and S. Adam, *Theoretical determination of the effect of a screening gate on plasmon-induced superconductivity in twisted bilayer graphene*, Phys. Rev. B **109**, 045404 (2024).

[19] E. Khalaf, S. Chatterjee, N. Bultinck, M. P. Zaletel, and A. Vishwanath, *Charged skyrmions and topological origin of superconductivity in magic-angle graphene*, Sci. Adv. **7**, eabf5299 (2021).

[20] Y. H. Kwan, G. Wagner, N. Bultinck, S. H. Simon, and S. A. Parameswaran, *Skyrmions in twisted bilayer graphene: stability, pairing, and crystallization*, Phys. Rev. X **12**, 031020 (2022).

[21] J. González and T. Stauber, *Kohn-Luttinger superconductivity in twisted bilayer graphene*, Phys. Rev. Lett. **122**, 026801 (2019).

[22] M. Long, A. Jimeno-Pozo, H. Sainz-Cruz, P. A. Pantaleón, and F. Guinea, *Evolution of superconductivity in twisted graphene multilayers*, Proc. Natl. Acad. Sci. U.S.A. **121**, e2405259121 (2024).

[23] M. Christos, S. Sachdev, and M. S. Scheurer, *Nodal band-off-diagonal superconductivity in twisted graphene superlattices*, Nat. Commun. **14**, 7134 (2023).

[24] T. J. Peltonen, R. Ojajärvi, and T. T. Heikkilä, *Mean-field theory for superconductivity in twisted bilayer graphene*, Phys. Rev. B **98**, 220504(R) (2018).

[25] F. Wu, A. H. MacDonald, and I. Martin, *Theory of phonon-mediated superconductivity in twisted bilayer graphene*, Phys. Rev. Lett. **121**, 257001 (2018).

[26] Y. W. Choi and H. J. Choi, *Strong electron-phonon coupling, electron-hole asymmetry, and nonadiabaticity in magic-angle twisted bilayer graphene*, Phys. Rev. B **98**, 241412(R) (2018).

[27] F. Wu, E. Hwang, and S. Das Sarma, *Phonon-induced giant linear-in- T resistivity in magic angle twisted bilayer graphene: Ordinary strangeness and exotic superconductivity*, Phys. Rev. B **99**, 165112 (2019).

[28] B. Lian, Z. Wang, and B. A. Bernevig, *Twisted bilayer graphene: A phonon-driven superconductor*, Phys. Rev. Lett. **122**, 257002 (2019).

[29] M. Kim *et al.*, *Control of electron-electron interaction in graphene by proximity screening*, Nat. Commun. **11**, 2339 (2020).

[30] H. Schmidt, T. Lüdtke, P. Barthold, E. McCann, V. I. Fal'ko, and R. J. Haug, *Tunable graphene system with two decoupled monolayers*, Appl. Phys. Lett. **93**, 172108 (2008).

[31] G. Li, A. Luican, and E. Y. Andrei, *Scanning tunneling spectroscopy of graphene on graphite*, Phys. Rev. Lett. **102**, 176804 (2009).

[32] J. D. Sanchez-Yamagishi, T. Taychatanapat, K. Watanabe, T. Taniguchi, A. Yacoby, and P. Jarillo-Herrero, *Quantum Hall effect, screening, and layer-polarized insulating states in twisted bilayer graphene*, Phys. Rev. Lett. **108**, 076601 (2012).

[33] Y. Kim *et al.*, *Breakdown of the interlayer coherence in twisted bilayer graphene*, Phys. Rev. Lett. **110**, 096602 (2013).

[34] J. D. Sanchez-Yamagishi, J. Y. Luo, A. F. Young, B. M. Hunt, K. Watanabe, T. Taniguchi, R. C. Ashoori, and P. Jarillo-Herrero, *Helical edge states and fractional quantum Hall effect in a graphene electron–hole bilayer*, Nat. Nanotechnol. **12**, 118 (2017).

[35] Y. Wang, J. Zhu, G. W. Burg, A. Swain, K. Watanabe, T. Taniguchi, Y. Zheng, A. H. MacDonald, and E. Tutuc, *Independently tunable flat bands and correlations in a graphene double moiré system*, Phys. Rev. Lett. **134**, 096204 (2025).

[36] J. C. Hoke, Y. Li, J. May-Mann, K. Watanabe, T. Taniguchi, B. Bradlyn, T. L. Hughes, and B. E. Feldman, *Uncovering the spin ordering in magic-angle graphene via edge state equilibration*, Nat. Commun. **15**, 4321 (2024).

[37] I. Babich *et al.*, *Milli-Tesla quantization enabled by tuneable Coulomb screening in large-angle twisted graphene*, Nat. Commun. **16**, 7389 (2025).

[38] See Supplemental Material at http://link.aps.org/supplemental/10.1103/z9qg-287y which includes Refs. [39–82].

[39] S. G. Xu *et al.*, *Giant oscillations in a triangular network of one-dimensional states in marginally twisted graphene*, Nat. Commun. **10**, 4008 (2019).

[40] X. Lu *et al.*, *Multiple flat bands and topological Hofstadter butterfly in twisted bilayer graphene close to the second magic angle*, Proc. Natl. Acad. Sci. U.S.A. **118**, e2100006118 (2021).

[41] J. M. B. Lopes dos Santos, N. M. R. Peres, and A. H. Castro Neto, *Graphene bilayer with a twist: Electronic structure*, Phys. Rev. Lett. **99**, 256802 (2007).

[42] R. Krishna Kumar *et al.*, *High-temperature quantum oscillations caused by recurring Bloch states in graphene superlattices*, Science **357**, 181 (2017).

[43] J. Barrier *et al.*, *Long-range ballistic transport of Brown-Zak fermions in graphene superlattices*, Nat. Commun. **11**, 5756 (2020).

[44] X. Wang *et al.*, *Moiré band structure engineering using a twisted boron nitride substrate*, Nat. Commun. **16**, 178 (2025).

[45] D. S. Kim *et al.*, *Electrostatic moiré potential from twisted hexagonal boron nitride layers*, Nat. Mater. **23**, 65 (2024).

[46] M. Yankowitz, S. Chen, H. Polshyn, Y. Zhang, K. Watanabe, T. Taniguchi, D. Graf, A. F. Young, and C. R. Dean, *Tuning superconductivity in twisted bilayer graphene*, Science **363**, 1059 (2019).

[47] S. Slizovskiy, A. Garcia-Ruiz, A. I. Berdyugin, N. Xin, T. Taniguchi, K. Watanabe, A. K. Geim, N. D. Drummond, and V. I. Fal'ko, *Out-of-plane dielectric susceptibility of graphene in twistronic and Bernal bilayers*, Nano Lett. **21**, 6678 (2021).

[48] P. Moon and M. Koshino, *Optical absorption in twisted bilayer graphene*, Phys. Rev. B **87**, 205404 (2013).

[49] S. Carr, D. Massatt, S. B. Torrisi, P. Cazeaux, M. Luskin, and E. Kaxiras, *Relaxation and domain formation in incommensurate two-dimensional heterostructures*, Phys. Rev. B **98**, 224102 (2018).

[50] M. Xie and A. H. MacDonald, *Nature of the correlated insulator states in twisted bilayer graphene*, Phys. Rev. Lett. **124**, 097601 (2020).

[51] M. Koshino, Noah F. Q. Yuan, T. Koretsune, M. Ochi, K. Kuroki, and L. Fu, *Maximally localized Wannier orbitals and the extended Hubbard model for twisted bilayer graphene*, Phys. Rev. X **8**, 031087 (2018).

[52] N. Bultinck, E. Khalaf, S. Liu, S. Chatterjee, A. Vishwanath, and M. P. Zaletel, *Ground state and hidden symmetry of magic-angle graphene at even integer filling*, Phys. Rev. X **10**, 031034 (2020).

[53] R. Chatterjee, N. Rana, R. A. Simha, P. Perlekar, and S. Ramaswamy, *Inertia drives a flocking phase transition in viscous active fluids*, Phys. Rev. X **11**, 031063 (2021).

[54] I. Yudhistira, N. Chakraborty, G. Sharma, Derek Y. H. Ho, E. Laksono, O. P. Sushkov, G. Vignale, and S. Adam, *Gauge-phonon dominated resistivity in twisted bilayer graphene near magic angle*, Phys. Rev. B **99**, 140302(R) (2019).

[55] J. Bardeen, L. N. Cooper, and J. R. Schrieffer, *Theory of superconductivity*, Phys. Rev. **108**, 1175 (1957).

[56] J.-H. Chen, C. Jang, S. Xiao, M. Ishigami, and M. S. Fuhrer, *Intrinsic and extrinsic performance limits of graphene devices on* SiO_2, Nat. Nanotechnol. **3**, 206 (2008).

[57] D. K. Efetov and P. Kim, *Controlling electron-phonon interactions in graphene at ultrahigh carrier densities*, Phys. Rev. Lett. **105**, 256805 (2010).

[58] J. Berges, N. Girotto, T. Wehling, N. Marzari, and S. Poncé, *Phonon self-energy corrections: To screen, or not to screen*, Phys. Rev. X **13**, 041009 (2023).

[59] H. Bruus and K. Flensberg, *Many-Body Quantum Theory in Condensed Matter Physics: An Introduction* (Oxford University Press, Oxford, 2004).

[60] F. Marsiglio and J. P. Carbotte, *Electron—phonon superconductivity*, arXiv:cond-mat/0106143.

[61] M. Grabowski and L. J. Sham, *Superconductivity from nonphonon interactions*, Phys. Rev. B **29**, 6132 (1984).

[62] D. Scalapino, *Superconductivity*, edited by R. D. Parks (Marcel Dekker, Inc., New York, 1969), Vol. 1.

[63] G. Gladstone, M. Jensen, and J. Schrie, *Superconductivity*, edited by R. D. Parks (Marcel Dekker, Inc., New York, 1969), Vol. 1.

[64] J. S. Alden, A. W. Tsen, P. Y. Huang, R. Hovden, L. Brown, J. Park, D. A. Muller, and P. L. McEuen, *Strain solitons and topological defects in bilayer graphene*, Proc. Natl. Acad. Sci. U.S.A. **110**, 11256 (2013).

[65] Mohammed M. A. Ezzi, G. N. Pallewela, C. De Beule, E. J. Mele, and S. Adam, *Analytical model for atomic relaxation in twisted moiré materials*, Phys. Rev. Lett. **133**, 266201 (2024).

[66] Nguyen N. T. Nam and M. Koshino, *Lattice relaxation and energy band modulation in twisted bilayer graphene*, Phys. Rev. B **96**, 075311 (2017).

[67] A. Ramos-Alonso, B. Remez, D. Bennett, R. M. Fernandes, and H. Ochoa, *Flat and tunable moiré phonons in twisted transition-metal dichalcogenides*, Phys. Rev. Lett. **134**, 026501 (2025).

[68] C. D. Beule, G. N. Pallewela, M. M. A. Ezzi, L. Peng, E. J. Mele, and S. Adam, *Theory for lattice relaxation in marginal twist moirés*, Phys. Rev. B **113**, L241402 (2026).

[69] Nguyen N. T. Nam and M. Koshino, *Erratum: Lattice relaxation and energy band modulation in twisted bilayer graphene* [Phys. Rev. B **96**, 075311 (2017)]; **101**, 099901 (E) (2020).

[70] J. Kang and O. Vafek, *Analytical solution for the relaxed atomic configuration of twisted bilayer graphene including heterostrain*, Phys. Rev. B **112**, 125138 (2025).

[71] K. Uchida, S. Furuya, J.-I. Iwata, and A. Oshiyama, *Atomic corrugation and electron localization due to Moiré patterns in twisted bilayer graphenes*, Phys. Rev. B **90**, 155451 (2014).

[72] O. Vafek and J. Kang, *Continuum effective Hamiltonian for graphene bilayers for an arbitrary smooth lattice deformation from microscopic theories*, Phys. Rev. B **107**, 075123 (2023).

[73] J. Kang and O. Vafek, *Pseudomagnetic fields, particle-hole asymmetry, and microscopic effective continuum Hamiltonians of twisted bilayer graphene*, Phys. Rev. B **107**, 075408 (2023).

[74] C. De Beule, R. Smeyers, W. N. Luna, E. J. Mele, and L. Covaci, *Elastic screening of pseudogauge fields in graphene*, Phys. Rev. Lett. **134**, 046404 (2025).

[75] Z. Bi, Noah F. Q. Yuan, and L. Fu, *Designing flat bands by strain*, Phys. Rev. B **100**, 035448 (2019).

[76] M. M. A. Ezzi, L. Peng, Z. Liu, J. H. Z. Chao, G. N. Pallewela, D. Foo, and S. Adam, *A Self-Consistent Hartree theory for lattice-relaxed magic-angle twisted bilayer graphene*, arXiv:2404.17638.

[77] L. Peng, G. Vignale, and S. Adam, *Many-body perturbation theory for moiré systems*, Phys. Rev. B **112**, 075146 (2025).

[78] F. Marsiglio, *Eliashberg theory: A short review*, Ann. Phys. (Amsterdam) **417**, 168102 (2020).

[79] F. Ferreira, V. V. Enaldiev, and V. I. Fal'ko, *Scaleability of dielectric susceptibility ε_{zz} with the number of layers and additivity of ferroelectric polarization in van der Waals semiconductors*, Phys. Rev. B **106**, 125408 (2022).

[80] N. Ohba, K. Miwa, N. Nagasako, and A. Fukumoto, *First-principles study on structural, dielectric, and dynamical properties for three BN polytypes*, Phys. Rev. B **63**, 115207 (2001).

[81] J. Barrier *et al.*, *One-dimensional proximity superconductivity in the quantum Hall regime*, Nature (London) **628**, 741 (2024).

[82] M. Ben Shalom *et al.*, *Quantum oscillations of the critical current and high-field superconducting proximity in ballistic graphene*, Nat. Phys. **12**, 318 (2016).

[83] A. I. Berdyugin *et al.*, *Out-of-equilibrium criticalities in graphene superlattices*, Science **375**, 430 (2022).

[84] J. J. Hauser, H. C. Theuerer, and N. R. Werthamer, *Superconductivity in Cu and Pt by means of superimposed films with lead*, Phys. Rev. **136**, A637 (1964).

[85] A. G. Rojo, *Electron-drag effects in coupled electron systems*, J. Phys. Condens. Matter **11**, R31 (1999).

[86] J. P. Eisenstein and A. H. MacDonald, *Bose–Einstein condensation of excitons in bilayer electron systems*, Nature (London) **432**, 691 (2004).

[87] R. V. Gorbachev *et al.*, *Strong Coulomb drag and broken symmetry in double-layer graphene*, Nat. Phys. **8**, 896 (2012).

[88] K. F. Mak and J. Shan, *Semiconductor moiré materials*, Nat. Nanotechnol. **17**, 686 (2022).

[89] X. Gao *et al.*, *Double-edged role of interactions in superconducting twisted bilayer graphene*, Nat. Phys. **22**, 692 (2026).